Flux Lattice Melting and Dimensional Crossover in Bi-2212 Single Crystals

P. Kes, H. Pastoriza, T. Li, R. Cubitt, E. Forgan, S. Lee, M. Konczykowski, B. Khaykovich, D. Majer, D. Fuchs, et al.

J. Phys. I France 6 (1996) 2327-2354 DECEMBER 1996, PAGE 2327

Flux Lattice Melting and Dimensional Crossover in Bi-2212 Single Crystals

P.H. Kes ([1,*]), H. Pastoriza ([1]), T.W. Li ([1,**]), R. Cubitt ([2]), E.M. Forgan ([3]), S.L. Lee ([4]), M. Konczykowski ([5]), B. Khaykovich ([6]), D. Majer ([6]), D.T. Fuchs ([6]) and E. Zeldov ([6])

([1]) Kamerlingh Onnes Laboratory, Leiden University, P.O. Box 9506 2300 RA Leiden, The Netherlands

([2]) Institut Laue-Langevin, 38042 Grenoble Cedex 9, France

([3]) School of Physics and Space Research, University of Birmingham, Birmingham B15 2TT, UK

([4]) School of Physics and Astronomy, University of St. Andrews, North Haugh, St. Andrews, Scotland

([5]) Laboratoire des Solides Irradiés, École Polytechnique, 91128 Palaiseau, France

([6]) Department of Condensed Matter Physics, The Weizmann Institute of Science, 76100 Rehovot, Israel

(Received 14 June 1996, received in final form and accepted 26 August 1996)

PACS.74.60.Ec – Mixed state, critical fields, and surface sheath
PACS.74.60.Ge – Flux pinning, flux creep, and flux-line lattice dynamics
PACS.74.72.Hs – Bi-based cuprates

Abstract. — Flux lattice melting in $Bi_2Sr_2CaCu_2O_{8+x}$ (Bi-2212) single crystals has recently been studied by various techniques. In this contribution to the *I. Schegolev* Memorial Volume we review some experiments and compare their results. Muon-spin rotation and small angle neutron scattering (SANS) gave the first indications for an abrupt change of the flux lattice structure along a line in the $B-T$ phase diagram. Experiments with Hall-sensor arrays proved that the flux line lattice experiences a first order phase transition (FOT) at this line. Measured as a function of field the resistance shows an abrupt kink at the FOT line and flux flow through narrow channels reveals a sudden drop of the shear modulus. Subsequent studies showed that the location of the FOT line in the phase diagram strongly depends on oxygen stoichiometry. For decreasing temperature the FOT line terminates at a critical point and continues into an almost field independent line which represents the location of a sharp peak in the magnetization (second peak). The second-peak line coincides with a crossover region in the low temperature range of the $B-T$ diagram where both the muon spin rotation and SANS experiments reveal a transition from a lattice of flux lines to a lattice of pancake vortices. We compare our results with theoretical scenarios.

(*) Author for correspondence (e-mail: kes@rulgm0.LeidenUniv.nl)

(**) This contribution is mainly based on chapter 7 of the Ph.D. Thesis of T.W. Li (Leiden, 1995) and on references [36, 38, 39, 65, 73, 76].

1. Introduction

In many aspects the behavior of the high-T_c superconductors in the mixed state differs from that of conventional superconductors [1–10]. A combination of elevated critical temperatures, short superconducting coherence lengths and high anisotropy enormously enhance the role of thermal fluctuations on the vortex lines, which result in a noticeable change in the nature of the mixed state [11–14]. The nature of the flux lattice structures and the thermodynamic transition between the different vortex states has become one of the central questions of the physics of the mixed state and has attracted a great deal of attention [15–18].

The most important effect of thermal fluctuations is the possible melting of the vortex lattice at temperatures well below the critical temperature T_c [19, 20]. This phenomenon was studied for the 3D case using the Lindemann criterion [21–23]. In the pure 2D case dislocation-mediated melting takes place [24–27]. In 1988, Gammel and Bishop [28,29] made a controversial suggestion on the basis of high-Q mechanical oscillator data to explain the anomalous behavior of the HTS at high temperature. They suggested that the high temperature regime was a vortex liquid separated from the low temperature vortex lattice by a melting transition. The vortex-liquid phase is expected to occupy a significant part of the $B - T$ phase diagram [30]. On the other hand, the large anisotropy of Bi-2212 tends to confine the supercurrents to the CuO_2 planes, in which they form pancake vortices. There are attractive interactions between pancake vortices in different planes, so that they tend to line up, giving essentially three-dimensional flux line behavior. Upon increasing the flux density to a point where the shear interaction between the pancake vortices in the same layer becomes stronger than the tilt interaction between pancake vortices in adjacent layers, the presence of pinning can break up any order in the field direction, leading to a dimensional crossover from three-dimensional flux line behavior to two-dimensional behavior. When thermal fluctuations become large, melting of 2D point-vortex lattice in the CuO_2 planes of Bi-2212 does occur [31].

A first-order melting transition of the Abrikosov vortex lattice due to thermal fluctuations was predicted in 1985 by Brezin *et al.* [32]. It was suggested that the mean field formation of the vortex lattice at H_{c2}, that occurs *via* a thermodynamic second-order transition, can be driven into a first order transition by the superconducting fluctuations. In view of that result one may expect that in sufficiently clean crystals the vortex liquid freezes into an ordered solid through a thermodynamic first-order phase transition. The first experimental indication appeared in the compound $YBa_2Cu_3O_{7-x}$, when the behavior in clean twin-free samples was examined and hysteresis loops in the resistivity as a function of field and temperature were observed [33, 34], providing strong evidence for a first-order transition. However, it was argued [35, 36] that the resistivity is a dynamic quantity sensitive to pinning by the residual disorder present even in clean samples, and is not a thermodynamic property. A true first-order phase transition should have a clear thermodynamic fingerprint: a latent heat and a discontinuous step in the specific volume or density. Recently, such a first-order melting transition was observed by global magnetic measurements [37] and by local magnetic measurements [36] in Bi-2212 single crystals.

In this brief review we give an account of various investigations concerning the flux lattice structure in Bi-2212 single crystals as a function of both field and temperature. The main results were obtained from internal probes like muon spin rotation [38] and small-angle neutron scattering [39], and from external but local probes, *i.e.* Hall-sensor arrays [40]. Important additional information was provided by transport measurements. A study of the line shapes as a function of temperature and magnetic field using the muon spin rotation technique shows evidence for an abrupt change of the flux lattice structure which is attributed to the presence of a flux lattice melting line in the $B - T$ phase diagram. The data also suggest the existence

of a crossover field above which the flux structure attains a more two-dimensional (2D) nature.

Using small-angle neutron diffraction the flux line lattice inside a Bi-2212 single crystal was observed for the first time. The diffraction intensity shows a rapid decrease to zero at a magnetic field-dependent flux lattice melting temperature. The flux lattice signal is also shown to disappear at low temperatures by applying a sufficiently high field. This is probably due to the decomposition of flux lines into two-dimensional pancake vortices, in accord with the muon spin rotation results.

A thermodynamic first-order vortex lattice melting transition in Bi-2212 single crystal was observed at low fields by investigation of the local vortex density using microscopic Hall-sensor arrays. This first-order phase transition terminates at a critical point. Below the critical point, a second magnetization peak develops which is possibly connected to a 3D to 2D phase transition. The location of these two transition lines in the $B - T$ plane strongly depends on the oxygen stoichiometry.

2. Muon Spin Rotation Studies

An almost ideal tool for studying a nearly perfect flux line lattice is muon-spin rotation (μ^+SR). μ^+SR experiments in principle yield the field density distribution $p(B)$ inside bulk specimens [41, 42]. Such measurements were performed by Lee *et al.* [38] at the Paul Scherrer Institute, Switzerland, on high quality single crystals of Bi-2212. The crystals were grown by the Traveling Solvent Floating Zone (TSFZ) method [43]. They have a T_c of 84 K as determined by magnetization measurements. The sample consisted of a mosaic of eight large single crystals, each typically $5 \times 5 \times 0.5$ (mm^3), with the crystallographic c direction parallel to the shortest dimension and mounted perpendicular to the surface of an Fe_2O_3 plate. A magnetic field was applied parallel to the c-axis of the crystals and positive muons were incident on the sample with their spin-polarization vector perpendicular to the applied field. Time-differential μ^+SR spectroscopy was employed to determine the local internal field.

2.1. Results and Discussion. — Figure 1a shows the probability distribution of the local internal field $p(B)$ for the sample at a temperature of 5 K after cooling in an applied field of 52 G. The field distribution was obtained from a Fourier transform of the muon time spectrum using a maximum entropy technique [44]. This line shape shows features which are clear indications of a 3D flux structure [45], notably the long "tail" at fields higher than the applied, which arises from regions close to the vortex cores. This is the first clear observation of a 3D flux lattice line shape in Bi-2212 single crystals. The line shape could be well reproduced by a theoretical simulation taking $\lambda_{ab} = 180$ nm for the penetration depth and convoluting the field distribution of a perfect vortex lattice with a Gaussian of width 2.4 G to simulate the effects of lattice imperfection and instrumental resolution [38].

Figure 1b shows the distribution found for the sample at 54 K after cooling in an applied field of 454 G, and a second line shape obtained after the sample had been warmed to a temperature of 63.8 K. The shape of the latter spectrum is clearly different, with a loss of the high-field tail, reflecting a marked change of vortex structure.

In order to quantify such changes a ratio was defined, derived from the third and second moments of the line shape as

$$\alpha = \frac{\langle (\Delta B)^3 \rangle^{1/3}}{\langle (\Delta B)^2 \rangle^{1/2}} \tag{1}$$

This α is a dimensionless measure of the asymmetry of the line shape, the variation of which reflects underlying changes in the vortex structure. In Figure 2a α is plotted as a function of temperature for an applied field of 454 G. Here it can be seen that α changes sign abruptly

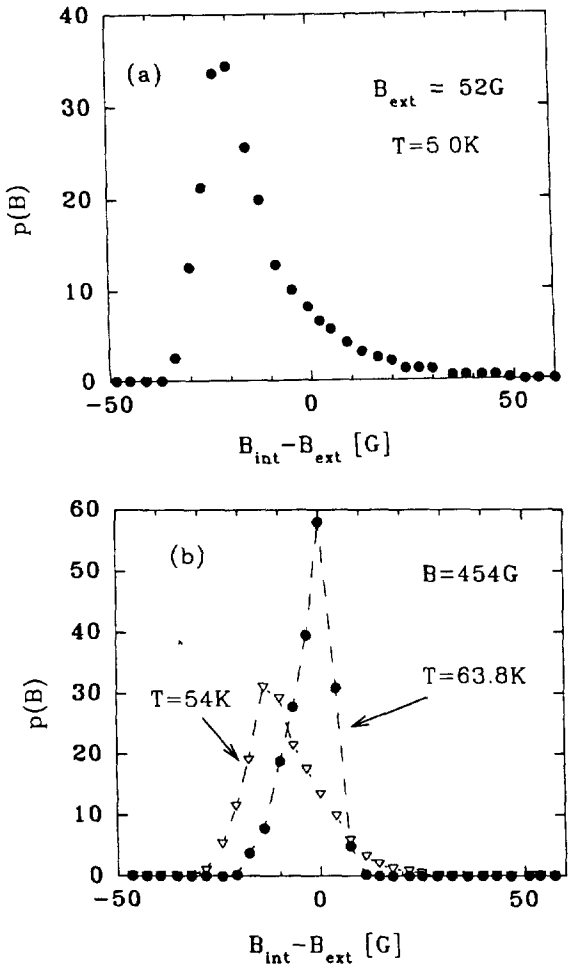

Fig. 1. — The probability distribution of the internal magnetic field in Bi-2212 crystals. a) At temperature 5 K and an applied field 52 G. The asymmetric line shape shows features which are a clear indication of a 3D flux structure. b) At an applied field 454 G and temperatures $T = 54$ K (triangles) and $T = 63.8$ K (circles) showing a significantly different line shape.

within a temperature range of less than 2 K, indicating the existence of a phase transition in the vortex structure. Moreover, the negative value of α obtained for the line shapes observed above the transition, reflects a substantial shift of probability away from the high-field tails. This is totally inconsistent with the existence of a triangular or square static 3D lattice. It is possible that the truncation of the high-field tail may reflect either a motion of the vortices [46] or a reduced dimensionality of the vortex structure [47], both of which could cause an effective smearing of the vortex cores. Plotted in Figure 2b is the temperature dependence of the second moment $\langle(\Delta B)^2\rangle$ of the field distribution. For a static array of 3D flux lines the second moment is a measure of superconducting penetration depth of the materials [48]. It follows from Figure 2b that the onset of the change of line shape, as indicated by the sudden decrease of the line-shape asymmetry in Figure 2a, is accompanied by a drop in the second moment from

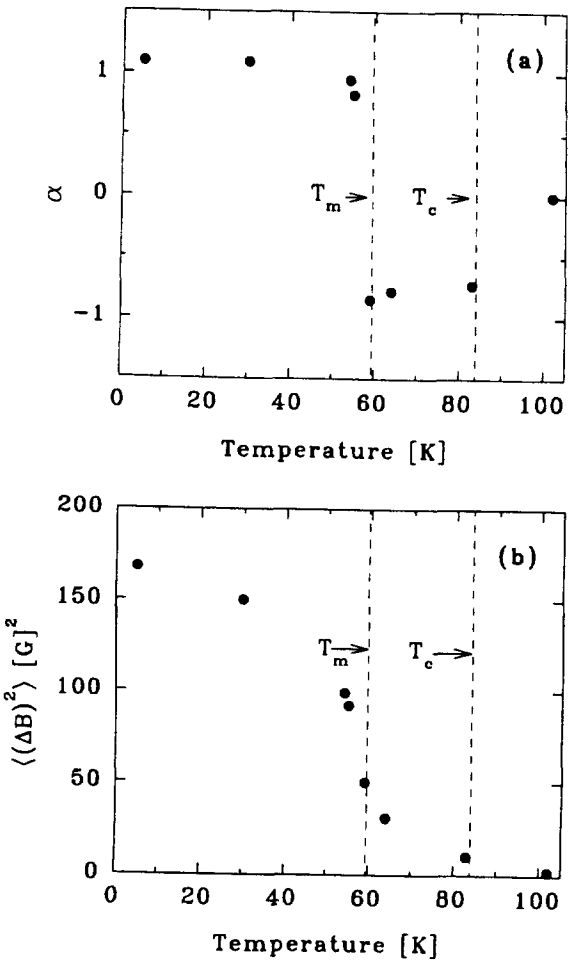

Fig. 2. — The temperature dependence of a) the asymmetry parameter α and b) the second moment of the field distribution after field cooling in 454 G. Note the sharp drop in the asymmetry of the line shape around $T_m = 59.5$ K and the simultaneous drop in the second moment at the same temperature.

the value expected by extrapolating the low-temperature behaviour $\langle(\Delta B)^2\rangle \propto \lambda^{-4}$. From the abruptness of the observed changes in the second moment and in α it is clear that there is a sharp transition of the vortex structure, which is associated with flux lattice melting.

Furthermore, this phase transition has been observed at several fields from 52 to 4010 G, and its temperature T_m has been ascertained with varying degrees of precision. The results are given in Figure 3 by the solid symbols. The origin of the solid line fitted to the data will be discussed in Section 4.2.

As discussed above, in highly anisotropic systems (like Bi-2212) the pancake vortices which are coupled by Josephson and magnetic interactions act as 3D line vortices at low fields. When the field is increased, the interaction between the pancake vortices in the same layer becomes stronger than between pancake vortices in adjacent layers leading to a dimensional crossover from 3D to 2D elastic behavior. It has been shown that disorder induced by random pinning in

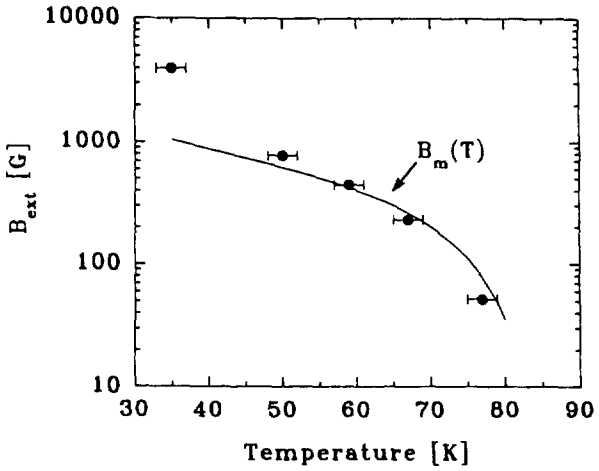

Fig. 3. — $B - T$ phase diagram showing the melting temperature as detected by the change in muon spin rotation line shape. The transition was defined as the onset of the change from a negative to a positive third moment of the field distribution, as indicated in Figure 2. The solid line is a fit of equation (9) to the three lowest field points, see Section 4.2 for further discussion.

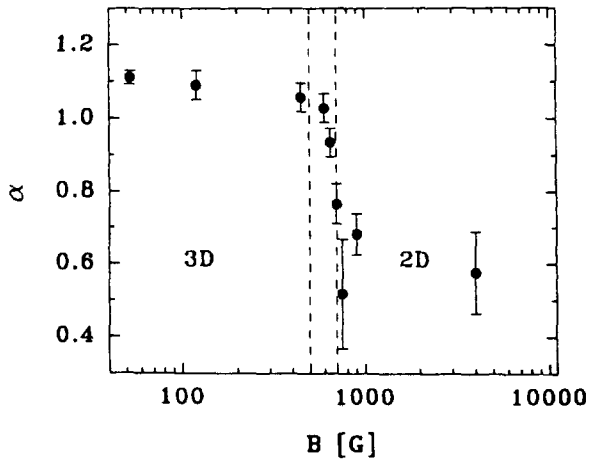

Fig. 4. — The field dependence of the asymmetry parameter α at $T = 5$ K after field cooling at each field. The large drop in magnitude beginning at B about 500 G is believed to reflect a crossover from a 3D flux line to a 2D pancake vortex structure. The crossover region is indicated by the vertical dashed lines.

such a system reduces the correlations between the positions of vortex cores in adjacent layers, and may truncate the high field tail. It also reduces the second moment and the asymmetry of the line shape, and causes the peak field to move towards the applied field [46, 47, 49]. In Figure 4 the low temperature value of the asymmetry parameter α, obtained in each case after field cooling the sample, is plotted as a function of field. The sharp drop of α beginning at about 500 G indicates a change of vortex structure with increasing field. An example of the

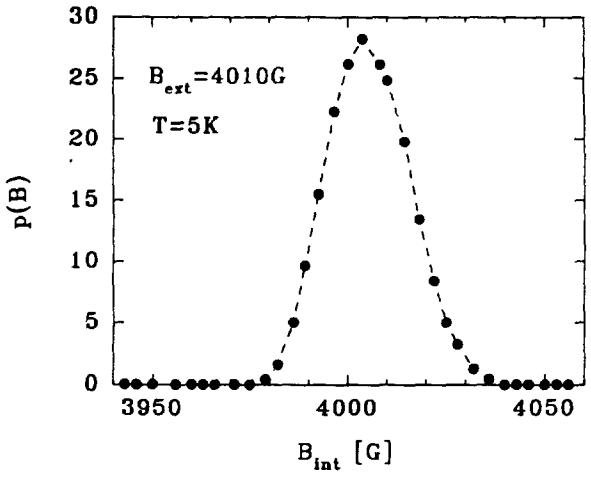

Fig. 5. — Typical line shape observed for fields above the field at which the asymmetry parameter α in Figure 4 drops sharply. Note the symmetrical line shape around a B value slightly below the applied field of 4010 G.

more symmetric line shape found above this field-induced transition is shown in Figure 5. It appears to be centered at a B-value which is just below the applied field. While one also observes a truncation of the high-field tail, the line shape is quite different from that observed in Figure 1b. Furthermore, in contrast to the transition at T_m, the low temperature transition in field involves only a change of magnitude, not of sign. Observation of similar high-field line shapes were taken by Harshman *et al.* [47] to indicate the presence of a 2D array of fluxons disordered along the c direction by random pinning. Since at low fields we have clear evidence for the existence of a 3D vortex structure, this strongly suggests that the transition is associated with the decomposition of flux lines into pancake vortices.

Such a crossover field B_{2D} is expected for a highly anisotropic system like Bi-2212 and may be estimated as that field where the average intervortex distance $R_{av} = a_0 \simeq (\Phi_0/B)^{1/2}$ becomes less than the Josephson length $R_J \simeq \gamma s$, where s is the separation of the superconducting layers, $\gamma = (m_c/m_{ab})^{1/2}$, and m_{ab} and m_c are the components of the anisotropic effective-mass tensor parallel and perpendicular to the ab plane, respectively [13]. Taking $s = 1.5$ nm and $\gamma = 150$ [50] yields $B_{2D} \simeq 400$ G. In the present data the onset of the change of flux structure occurs at about 500 G, which is in accordance with the above estimate for a crossover field. Further evidence for a dimensional cross-over comes from the temperature dependence of $\langle(\Delta B)^2\rangle$ above and below B_{2D}. At fields below B_{2D} the temperature dependence is anomalous, *i.e.* deviating from $\langle(\Delta B)^2\rangle \propto \lambda^{-4}$, only above T_m (see Fig. 2), while above B_{2D} the temperature dependence is anomalous across the whole temperature range, both above and below the transition temperature T_m [51]. This may reflect the increased importance of thermal fluctuations in the more weakly coupled layers [52]. Similar effect of thermal fluctuation in the Tl-2201 compound were reported by Schegolev *et al.* [14].

3. Small-Angle Neutron Diffraction

Neutron diffraction offers another internal probe to study the flux line structure. This technique, first suggested by De Gennes and Matricon [53], and put into practice by Criber *et al.*

in Nb [54], works by scattering neutrons from the small field modulations in the sample which are there because of the quantized flux lines of the mixed state. In much the same way as one can image lattices of atoms in crystals and obtain their structures. It is not like most other techniques which either do not image the lattice at all or do so in a way that is very limited as a function of temperature and field [1]. Small-angle neutron scattering (SANS) can image the lattices of magnetic flux lines in type II superconductors and directly obtain their structures as a function of temperature and applied magnetic field. The drawback is that the signals can be very weak, especially for materials such as the HTS which have large magnetic penetration depths. This is because the integrated scattered intensity I_{hk} for the (h,k) Bragg reflection is

$$I_{hk} \propto \frac{\mid F_{hk} \mid^2}{\sin\theta_{hk}} \tag{2}$$

where θ_{hk} is the Bragg angle for the (h,k) reflection with respect to the normal to the lattice planes and F is the "form factor", which is proportional to the magnitude of the field contrast. In type II superconductor with a large Ginsburg-Landau parameter, the effect of the flux line cores can be neglected unless the flux density B is close to the upper critical flux density B_{c2}, which would only apply close to T_c. The solution of the London equation leads to an explicit expression for F [55]:

$$F_{hk} = \frac{B}{1+(2\pi\lambda/d_{hk})^2} \tag{3}$$

where d_{hk} is the spacing between the (h,k) planes. The $(1,0)$ reflection, with the largest d-spacing, will have the greatest intensity. If $d_{10} \simeq a_0 < \lambda$, implying that $B > B_{c1}$, the second term in the denominator of equation (3) dominates, so that

$$I_{10} \propto d_{10}\frac{\Phi_0^2}{\lambda_{ab}^4} \tag{4}$$

Thus, for a given flux-line spacing, the scattered intensity would be greatly reduced in a material with a large penetration depth. If we compare the HTS with *e.g.* Nb, the low-temperature values of the penetration depths are greater than that of Nb by factors of at least four, *i.e.* Bi-2212, 200 nm, and Nb, 40 nm. Therefore the scattering signals in HTS are comparatively weak and a large single crystal is then essential.

The angle of diffraction depends on the flux line lattice spacing a_0 which is controlled by the flux density B, *i.e.* with an applied magnetic field of 500 G, $a_0 \simeq 200$ nm, which implies very small-angle scattering. This would have to be detected in the presence of additional scattering from twins, cracks or other inhomogeneities, and thus single crystals of high-quality are also essential.

Finally, this experiment also requires single crystals which have a very small mosaic spread along the direction of the incident neutron bundle, *i.e.* the field direction, because the observed scattering pattern is the sum of the patterns from each part of the crystal.

3.1. EXPERIMENT. — The neutron beam was provided by the cold source at the DR3 reactor, Risø, Denmark. The high quality Bi-2212 single crystals were grown by the TSFZ method [43]. The sample (which was a part of the μ^+SR sample) was a 180 mg plate-like crystal of Bi-2212 with its c-axis parallel (within one degree) to both an applied field and the incident neutron beam. The sample was mounted in a variable-temperature cryostat capable of cooling to 1.5 K. In this geometry, analogous to that employed for diffraction in a transmission electron microscope, the scattering vectors of the lattice are perpendicular to the beam. The SANS instrumentation allowed a 6 m collimating path for the beam before the sample, and a 6 m

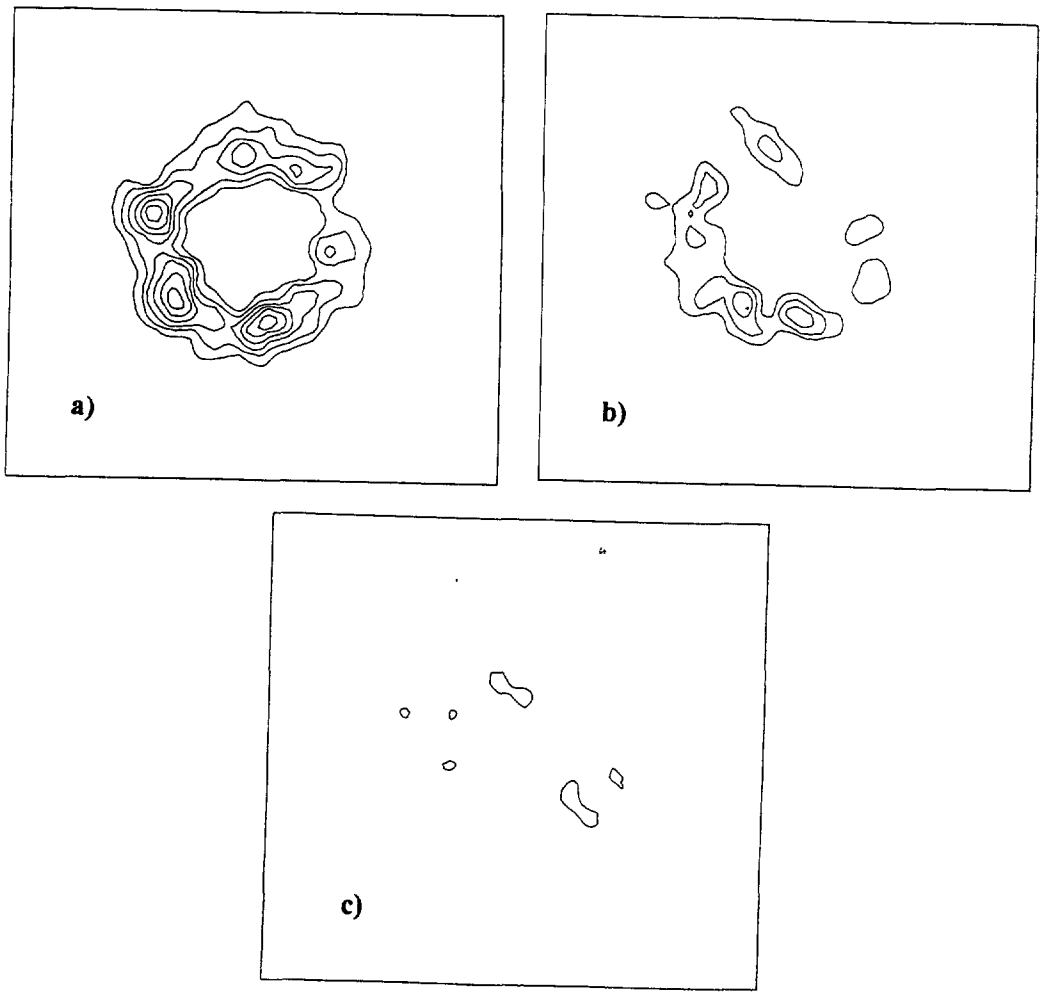

Fig. 6. — Diffraction patterns from the flux lattice in a Bi-2212 crystal at an applied magnetic field of 475 G at temperatures of a) 1.5 K, b) 56 K, and c) 62 K. The melting temperature was identified as 60 K at this field.

path from the sample to an area detector of 59 cm diameter with a resolution of 8 mm. At the lowest fields employed, 200 G, the flux line spacing is greater than 300 nm. An incident neutron wavelength λ_n of 1.95 nm, with a wavelength spread $\delta\lambda_n/\delta\lambda_n = 0.18$ full-width at half-maximum (FWHM), was used to give sufficiently large scattering angles. Details about the subtraction of background corrections can be found in reference [39].

3.2. Melting and Decomposition of Flux Lines. — A typical low-temperature diffraction pattern after subtraction and smoothing is shown in Figure 6a.

The axis of the beam is nearly parallel to the flux lines, so the diffraction spots are approximately equal in intensity [56]. Unlike YBCO under similar conditions [57], a hexagonal diffraction pattern is observed. On increasing the temperature of the sample, the diffraction intensity goes rapidly to zero at a temperature T_m which is much less than the T_c of 84 K.

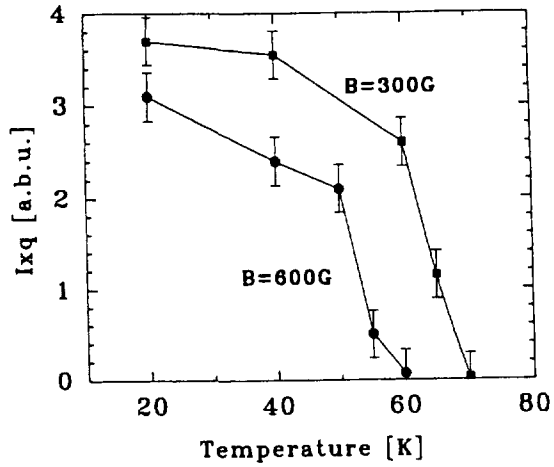

Fig. 7. — Temperature dependence of the integrated intensity of one of the spots in the diffraction pattern, multiplied by q_{hk}, which is proportional to the form factor. Data are shown at applied fields of 300 and 600 G.

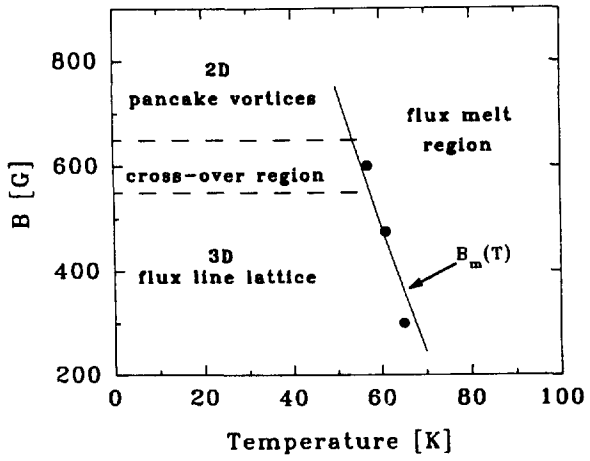

Fig. 8. — $B - T$ phase diagram from the neutron scattering data. The solid line is a fit of the expression for the melting line, equation (9), to these data, see discussion in Section 4.2.

Typical diffraction patterns as a function of temperature are shown in Figure 6. The results of temperature scans at two different applied fields are shown in Figure 7. It is clearly shown that T_m decreases with increasing B. In Figure 8 three values for T_m are plotted in the $B - T$ plane.

Within the accuracy of our data no pre-melting phenomena such as a change in the width of the spots are seen as the temperature is increased, only a fall in intensity. Above the melting transition any diffraction intensity is too small to measure in this experiment. There is no ring of intensity, as would be expected for a liquid array of rod-like flux lines. We believe that this is because the flux lines are not sufficiently straight in the liquid state. Using an expression for

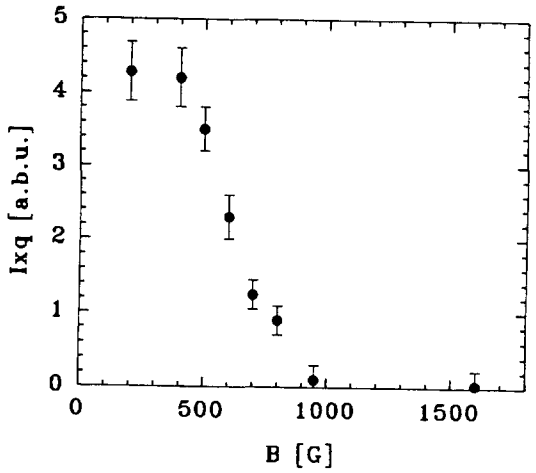

Fig. 9. — Applied-field dependence of the integrated intensity (at 1.5 K) of one of the spots in the diffraction pattern multiplied by q_{hk} to give a quantity proportional to the form factor.

the tilt modulus c_{44} [58], and bearing in mind that the shear modulus c_{66} is zero in the liquid state, we may estimate the energy to tilt a flux line by some fraction δa_0 of the flux lattice parameter a_0, to form a kink of length L_z, namely

$$E_{\text{tilt}} \simeq \epsilon_0 \frac{(\delta a_0)^2}{\gamma^2 L_z} \tag{5}$$

where $\epsilon_0 = (\Phi_0/4\pi\lambda_{ab})^2$. Taking an extreme case of $\delta a_0/L_z = 1$ and $L_z = a_0$, we find this energy is equivalent to a temperature of 13 K at $B = 500$ G. This model calculation leads us to expect that the flux lines will not be straight after the flux lattice has melted. Indeed, on increasing temperature and field the flux structure will eventually turn into a two-dimensional liquid pancake mix [59], if it does not already form it on melting.

We now turn to the variation of the diffraction signal at low temperature as a function of increasing field. As always, the new structure is formed by cooling through T_c in an applied field. We find that the signal disappears rapidly with the midpoint of the transition at about 650 G. It is shown in Figures 9 and 10. The intensity of the spots is reduced in a similar manner to the temperature transition, although not quite so sharply. Related phenomena have been observed in the μ^+SR data [38], and we ascribe this to a dimensional crossover in pinning, which leads to a static arrangement of pancake vortices with little alignment in the field direction. According to the collective-pinning theory of Larkin and Ovchinnikov, the length of a coherently pinned volume V_c is $(c_{44}/c_{66})^{1/2}$ multiplied by its extent perpendicular to the field.

In Bi-2212, it is believed that flux lines are pinned individually at fields below 5 T and temperature below 15 K [60], so the perpendicular extent should be taken as a_0 and the short-wavelength form of c_{44} should be used, which is extremely "soft". Using the expression in references [13, 58], we find that

$$\frac{c_{44}}{c_{66}} \simeq \frac{B^2}{\mu_0 \lambda_c (\pi/a_0)^2} \Big/ \frac{B\Phi_0}{16\pi\mu_0\lambda_{ab}^2} \simeq \frac{16}{\pi\gamma^2} \tag{6}$$

Simple substitutions show that the pinning length becomes comparable with the inter-CuO_2 plane separation s as the field is raised above $B_{2D} \simeq \Phi_0/(\gamma s)^2$, which is about 400 G for

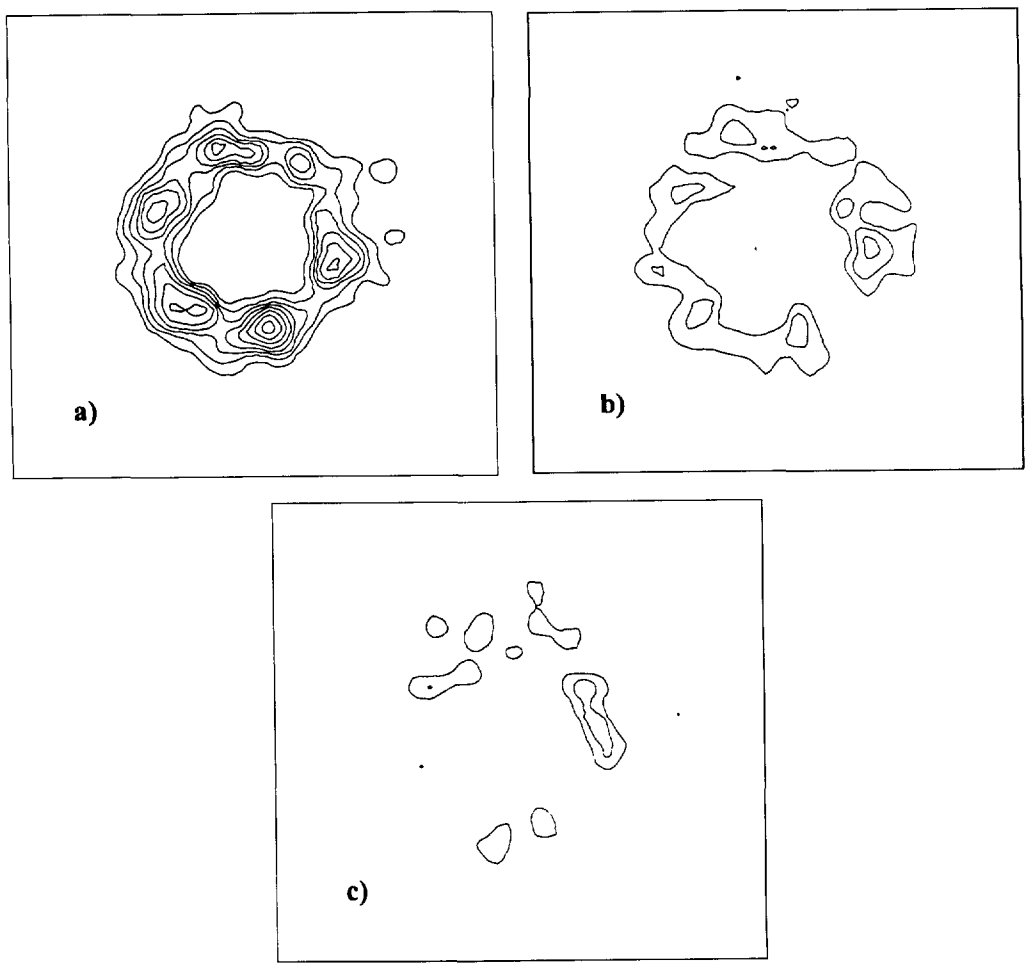

Fig. 10. — Diffraction patterns from the flux lattice in Bi-2212 at temperature 1.5 K and an applied magnetic field (a) 500 G, (b) 700 G and (c) 950 G.

$s = 1.5$ nm and $\gamma = 150$. In view of the crudeness of our estimate of B_{2D}, this value is in sufficiently good agreement with the observed crossover field.

Further measurements below the melting line indicate that the crossover field B_{2D} is approximately temperature-independent. According to the μ^+SR measurements, melting also occurs well above 650 G. Presumably this is two-dimensional melting, but the absence of a detectable diffraction signal indicates that the flux line structure is far too disordered in this region to be investigated by means of neutron diffraction.

At lower fields, in the flux lattice state, the total intensity I_{hk} of a single diffraction spot, obtained by integrating over angle as the sample is rocked through the Bragg condition (rocking curve for the hk reflection), is given by the formula [61]:

$$I_{hk} = 2\pi\varphi\left(\frac{\mu}{4}\right)^2 \frac{V\lambda_n^2}{\Phi_0^2 q_{hk}} \mid F_{hk} \mid^2 \tag{7}$$

where φ is the incident neutron flux/m^2, μ is the magnetic moment of the neutron in nuclear magnetons. For rigid flux lines, the London theory gives equation (3) with $q_{hk} = 2\pi/d_{hk}$ where q_{hk} is the scattering vector.

A loss of intensity at a given sample orientation could arise either from a reduction in the form factor F_{hk} or an increase in the width of the rocking curve. The low-temperature rocking curves were measured both at 500 G and at 650 G. In the latter case the intensity is a factor of 3.6 below that found at 500 G. In both cases the FWHM of the rocking curve was 1.2° indicating that only the form factor had changed. We believe that above B_{2D} the short length scale of the pinning in the c direction means that individual pancakes can be pinned away from the flux line axis reducing the field contrast in the mixed state. Using the equations for the diffraction intensity and the form factor to calculate a value for λ_{ab} from spot intensities observed at 500 G and 1.5 K, a value of 210 nm was obtained. This should be regarded as an upper limit, due to the effects of any disorder of the flux lattice on the diffraction intensity. This value is similar to that found by μ^+SR.

4. First-Order Vortex Lattice Melting Transition

Although the μ^+SR and SANS experiment clearly indicate that there is a vortex-lattice melting transition in Bi-2212 well below T_c, it remains to be seen whether this transition is a real first, or second order phase transition. Especially, a first order (phase) transition (FOT) can be recognized by a latent heat and a finite step in flux density. The first experiment to provide unambiguous evidence for a FOT was recently carried out by Zeldov *et al.* [36] on an as-grown Bi-2212 single crystal. Because the oxygen content is so crucial for such properties as the penetration depth λ and the anisotropy γ, it is expected that the position of the FOT line in the B,T plane will depend on oxygen stoichiometry. Therefore further experiments were carried out on several Bi-2212 single crystals which received different anneal treatments. In addition, the effect of oxygen content on the second peak in the irreversible magnetization curve was investigated.

4.1. EXPERIMENT. — In order to probe the true width of the phase transition, one needs to make local measurements with high spatial resolution. For this purpose, an array of 11 GaAs/AlGaAs two-dimensional-electron-gas Hall sensors with an active area of 10×10 μm^2 each was used. The sample was put directly onto the surface of the sensors and a perpendicular external magnetic field H_a was aligned along the crystallographic c-axis. The Hall-sensor array allows the study of local vortex behavior with high field-sensitivity and high spatial resolution. An additional advantage of this technique is that one obtains the actual value of local B. In global magnetization measurements only the value of the applied field H_a is known, and an accurate determination of B is difficult due to complicated demagnetization effects. In a standard global magnetization measurement the signal is integrated over the entire sample which results in significantly broader and smoother features as compared to the underlying physical mechanism. This is because the magnetic induction B inside a platelet crystal is not uniform even at equilibrium magnetization [62, 63]. As a result, the vortex lattice melting transition at various positions inside the superconducting sample occurs at slightly different temperatures or applied fields which smears out the transition.

The experiments were performed on two Bi-2212 single crystals grown by the TSFZ method [43]. These two crystals have different oxygen contents after annealing in air at 500 and 800 °C and will be referred to as Bi1 and Bi2, respectively. Bi1 is in the overdoped regime and has $T_c = 84.5$ K and $\lambda = 180$ nm, while Bi2 is optimally doped with $T_c = 89$ K and $\lambda = 240$ nm [64].

4.2. Results and Discussion

4.2.1. Melting Transition. — Figure 11 shows typical local magnetization loops as measured by the Hall sensors for Bi1 and Bi2 at 70 K and for the as-grown crystal [66] at 64 K. The first order transition (FOT) is clearly seen as a jump in the equilibrium magnetization. As has been seen before [37], B in the liquid is larger than in the vortex-solid. That is, the vortex liquid expands upon freezing, similar to the transformation of water into ice. Such behavior is rare in nature and shows that matter composed of flexible directed lines with long range interaction behaves differently from assemblies of point-like atoms or molecules. In such systems of line objects the gain in entropy due to entanglement overrules the energy increase related to the higher density of the liquid [67].

The first-order phase transition has been observed and measured at different temperatures between 40 and 80 K for both Bi1 and Bi2. Compared to the results on as-grown crystals, the width of the transition is slightly broader and the step height ΔB is smaller being about 0.1-0.2 G instead of 0.4 G. A possible explanation is that the present experiments were carried out with Hall sensors with an active area of 10×10 μm^2 whereas in reference [36] an array with sensors of 3×3 μm^2 was used. The sensors with a larger active area will make the melting transition look much wider. On the other hand, annealing and quenching the sample may introduce more disorder in the crystal, which will also smear the transition. The results of the as-grown crystals are therefore better suited for thermodynamic considerations, which will be given below. We first concentrate on the position of the FOT lines in the B, T plane.

The resulting FOT data, as defined by the mid-points of the jumps, are collected in Figure 12a for single crystals of different oxygen content. The influence of the oxygen stoichiometry is clearly seen. At the same temperatures the FOT fields of the overdoped sample (Bi1) are much larger than for the optimally doped sample (Bi2). The data for the as-grown crystal lies near that of Bi2 revealing that the as-grown material is close to optimal doping. The FOT terminates abruptly at a sample dependent temperature in the range between 40 and 50 K, indicated by the arrow.

The data of Pastoriza *et al.* [37] would also lie between the optimally and overdoped results. According to the experiment, these data represent the decoupling line at which a vortex line liquid decomposes into uncorrelated pancake vortices [59]. Daemen *et al.* [68] argue that the decoupling line would most likely be a FOT. Obviously, another scenario for the FOT is vortex lattice melting. To study the latter possibility in more detail one can try to fit the theoretical expression for the melting line of a 3D vortex lattice [20, 21] to the data of Bi1 and Bi2. This expression is based on the Lindemann criterion and is given by

$$B_{3D}(T) \simeq \frac{1}{64\pi^3}\{\frac{\Phi_0^5 c_L^4}{(\gamma k_B T_c \lambda_{ab}^2(0))^2}\}\{\frac{1-(T/T_c)^p}{T/T_c}\}^2 \tag{8}$$

where c_L is the Lindemann parameter, γ is the anisotropy parameter ($\gamma \gg 1$) and p is a parameter accounting for the temperature dependence of λ. With $p = 1$ we have the Ginsburg-Landau behavior, for $p = 4$ the two-fluid model. Reasonable results were obtained previously [38, 39] by fitting this formula to the data obtained with μ^+SR and SANS experiments on overdoped samples comparable to Bi1: The best fit was found for $c_L = 0.2$, $\gamma = 150$, $\lambda_{ab}(0) = 180$ nm, $p = 3.3$. Considering the larger transition temperature, penetration depth and lattice parameter of Bi2 (presumably giving a larger anisotropy) a much lower melting line is expected for Bi2, in agreement with Figure 12a. However, equation (8) was derived for the case of intermediate anisotropies for which the Josephson coupling between the layers is much larger than the electromagnetic coupling. For Bi-2212, with $\gamma > 150$ [50], the electromagnetic coupling can no longer be neglected. Recently, the melting behavior in highly anisotropic, layered

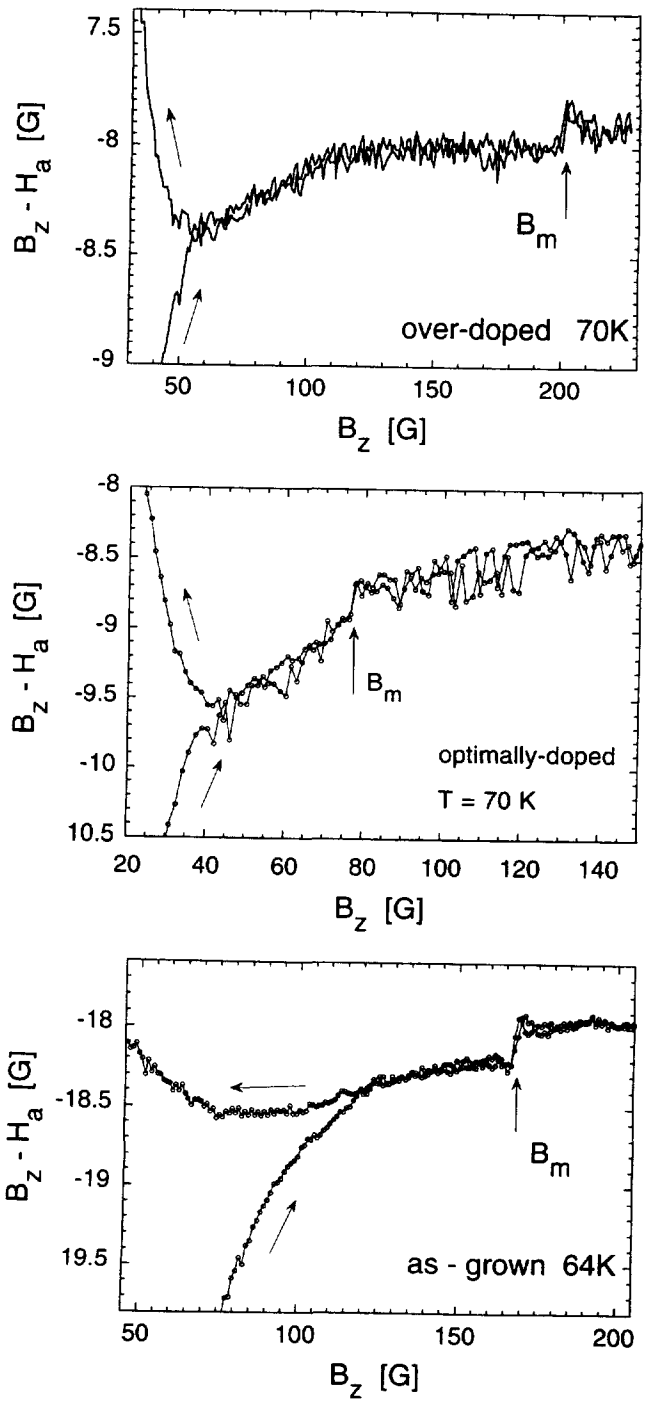

Fig. 11. — Local magnetization loops $B_z - H_a$ measured in the central part of BSCCO crystals as a function of the local magnetic induction for the over-doped (Bi1) and optimally-doped (Bi2) crystals at 70 K and an as-grown crystal [66] at 64 K. A first-order transition is manifested by a step in the reversible magnetization at B_m.

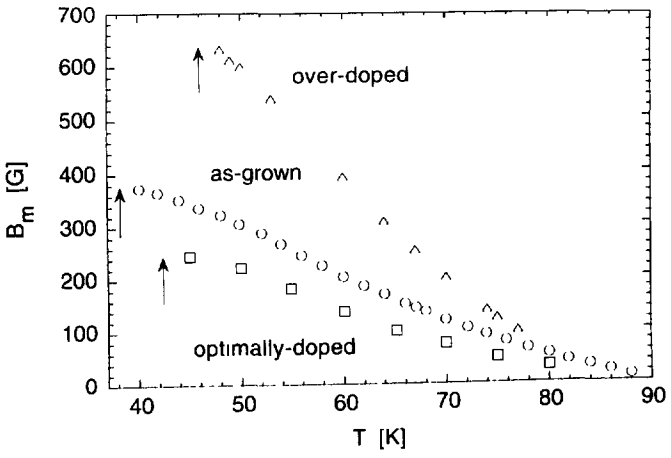

a)

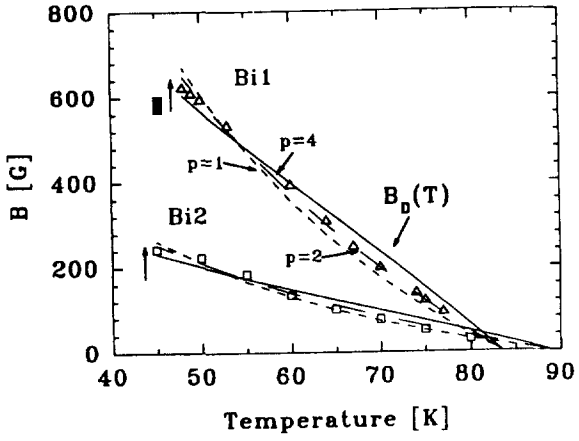

b)

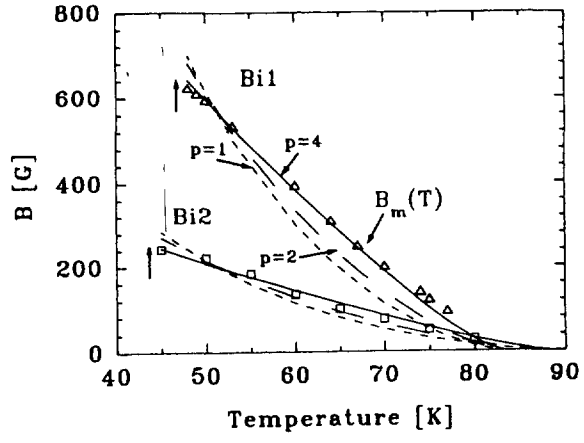

c)

Fig. 12. — a) The first-order transition for three BSCCO crystals of different anisotropy /oxygen content. The arrows indicate the temperature at which the step in the local induction abruptly terminates. In b) and c) the data of Bi1 and Bi2 are compared with the theoretical predictions for the decoupling line (Eq. (10)), and for a 3D melting line in the extreme anisotropic limit (sublimation line, Eq. (9)), respectively. For the temperature dependence of λ three possibilities were investigated: $p = 1$ represents the Ginzburg-Landau behavior, $p = 4$ the two-fluid behavior, and $p = 2$ some intermediate behavior. The fits were optimized for the anisotropy parameter γ. Results are summarized in Table I.

Table I. — *Anisotropy parameter γ determined from fits in Figures 12b and c.*

p	Melting, Eq. (9)		Decoupling, Eq. (10)	
	Bi1	Bi2	Bi1	Bi2
1	36	50	105	140
2	73	97	134	175
4	119	151	160	205

superconductors have been theoretically investigated taking both the electromagnetic and Josephson coupling into account [69]. In this case the melting line is determined by the new formula

$$B_{\mathrm{m}}(T) \simeq \frac{\Phi_0^3}{\gamma \lambda_{ab}^3(0)} \frac{c_I^2}{64\pi\sqrt{\beta}} \frac{1}{k_{\mathrm{B}} T} \left\{ 1 - \left(\frac{T}{T_{\mathrm{c}}} \right)^p \right\}^{3/2} \tag{9}$$

where $\beta = 1/\ln[1 + 4\lambda^2/(c_{\mathrm{L}} a_0)^2]$. This expression with $p = 1$, 2 and 4 has been fitted to the experimental data in Figure 12b, as well as in Figure 3 for the μ^+SR experiments and in Figure 8 for the neutron scattering experiments, both with $p = 4$. The fits were carried out with fixed values for the parameters c_{L} and β, *i.e.* $c_{\mathrm{L}} = 0.2$, $\beta \simeq 0.25$. Further, for Bi1 $T_{\mathrm{c}} = 83.5$ K and $\lambda_{ab} = 1800$ Å, and for Bi2 $T_{\mathrm{c}} = 89$ K and $\lambda_{ab} = 2400$ Å were substituted and the anisotropy was used as a free fit parameter. The dashed lines, denoting the $p = 1$ and $p = 2$ fits, clearly deviate from the data. The solid lines (two fluid model, $p = 4$) for Bi1 in Figures 3, 8 and 12b yields $\gamma \approx 151$. As is seen, the two-fluid model temperature dependence of λ yields the best fits to the data and also gives reasonable values of γ in comparison to the results of torque measurements [50]. Note that the optimally doped sample (Bi2) with the larger c-axis lattice parameter and the more semi-conducting behavior of the Bi-O layers, is expected to have the larger anisotropy. The anisotropies obtained from the fits for all p values are collected in Table I. Apart from the poor fits the γ values for $p = 1$ and $p = 2$ are unsatisfactorily low.

On the other hand, the decoupling line is expected to follow the expression [59]

$$B_{\mathrm{D}}(T) \simeq \frac{\alpha_{\mathrm{D}} \Phi_0^3}{16\pi^2 s k_{\mathrm{B}} T \gamma^2 \lambda_{ab}^2(0)} \left\{ 1 - \left(\frac{T}{T_{\mathrm{c}}} \right)^p \right\} \tag{10}$$

where $\alpha \approx 0.1$ is a universal parameter. In Figure 12c fits of this expression to the data are shown for $p = 1$, 2 and 4. The resulting γ values are given in Table I. It is seen that the quality of the fits is less sensitive to the precise temperature dependence of λ with a preference for $p = 2$. The resulting values of γ are reasonable, as well. We conclude that both the melting scenario (Eq. (9)) with $p = 4$ and the decoupling scenario (Eq. (10)) with $p = 2$ fit the data equally well. Therefore, experimentally it cannot be decided what is the physical origin of the first-order phase transition. Recent theoretical work [69] shows that for sufficiently large anisotropies the melting and decoupling line merge for fields below ϕ_0/λ^2. It might well be that this is the appropriate scenario for the FOT in Bi-2212.

4.2.2. Second Peak. — In the experiments of Khaykovich *et al.* [65] no discontinuous melting transition could be observed below the critical point. However, the local magnetization measurements show that an anomalous second peak appears at temperatures between 20 and 45 K. Such a second peak has also been reported for the Tl-2212 compound by Schegolev *et al.* [70]. The Bi-2212 results are shown in Figures 13a and b for one of the sensors in the center. We can clearly see that the peak field is strongly dependent on the oxygen content. As has been reported by Kishio *et al.* [71] it linearly increases with the oxygen concentration.

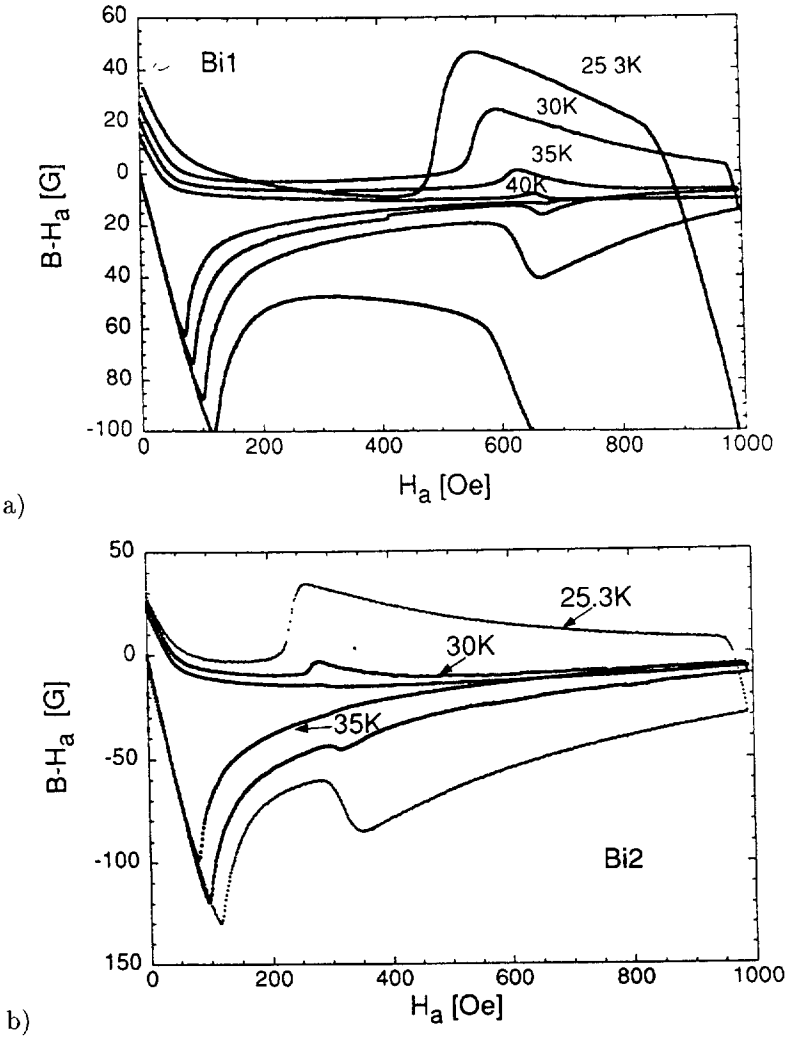

Fig. 13. — The local magnetization $B - H_a$ *vs.* the applied field H_a for a sensor situated in the center at constant temperatures (a) between 25.3 and 40 K for Bi1, (b) between 25.3 and 35 K for Bi2. It resembles the usual global magnetization curves showing the double peak structure.

With the Hall-sensor array the local field gradient dB_z/dx can be deduced by differentiating the field measured by adjacent sensors. In the second peak region the dB_z/dx drops sharply as the applied field H_a is decreased. This drop occurs at different values of H_a for various locations inside the crystal, starting from the edge and moving to the center due to the non-uniform field profile B_z. But, when the same data is plotted as a function of local induction B, the curves overlap. It means that the local magnetization sharply drops when the local field reaches the second peak field regardless of the position in the sample, indicating the thermodynamic nature of the underlying (phase) transition. The transition width is about 20 G. If smaller sensors are used, *i.e.* $3 \times 3\ \mu m^2$, a transition width of 5 G was observed. Therefore, the measured width is limited by the sensor size and the real transition width must be much narrower. The authors of [65] argue that the second peak is related to a second order phase-transition.

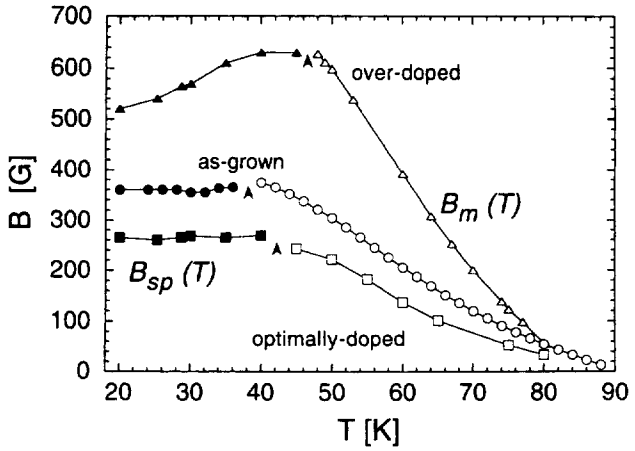

Fig. 14. — Low-field phase diagram for over-doped (Bi1), optimally doped (Bi2), and an as-grown sample [36]. The open symbols represent the first-order phase transition data, the arrows indicate the position of the critical point, and the solid symbols denote the positions of the second peak in the irreversible magnetization.

4.3. Low-field Phase Diagram. — The complete phase diagram for Bi1 and Bi2 in comparison to the previously published result for an as-grown sample [36] is given in Figure 14. It is seen that when the first-order transition terminates at the critical point, the second magnetization peak develops. The apparent interval in the data around the critical point in Figure 14 is due to the disappearance of the second magnetization peak at temperatures close to the critical point. The two lines meet at the critical point regardless of the differences between the samples which are related to the differences in anisotropy and penetration depths. This finding strongly suggests that these two lines actually represent one continuous vortex-lattice phase transition line.

In order to compare the results for all these independent experimental techniques, we now plot the $B - T$ phase diagram for Bi1 in Figure 15 and include the data obtained by neutron scattering and muon spin rotation experiments. It should be noted that the samples used in the μ^+SR and SANS experiments have the same composition and received the same heat treatment as Bi1. Their properties should therefore be identical. Comparing the data in Figure 15 one should keep in mind that for the neutron scattering experiments only the applied field is known. This is slightly larger than the local field, which is directly measured in the μ^+SR and Hall probe experiments and is plotted along the ordinate in Figure 15.

Figure 15 shows that the high-temperature results of the SANS and μ^+SR experiments coincide with the FOT line determined with the Hall sensors. This proves that the decrease of peak intensity (Sect. 3) and the sudden change of asymmetry in line shape (Sect. 2) indeed probe the same abrupt change in the vortex structure related to the FOT. The SANS observations are in agreement with a decoupling scenario, or a transition to a highly entangled flux line liquid. However, a liquid of fairly straight lines would give rise to SANS in a ring instead of the total disappearance of the intensity. If the FOT probes a melting transition, it thus can only be one in which the decomposition into pancakes takes place simultaneously in accord with recent theory [69]. This conclusion qualitatively agrees also with the ac susceptibility experiments of Pastoriza *et al.* [37], but a direct comparison with the results in Figure 15 is impossible, since the oxygen content of the sample used in [37] is not specified. The crossover line which is

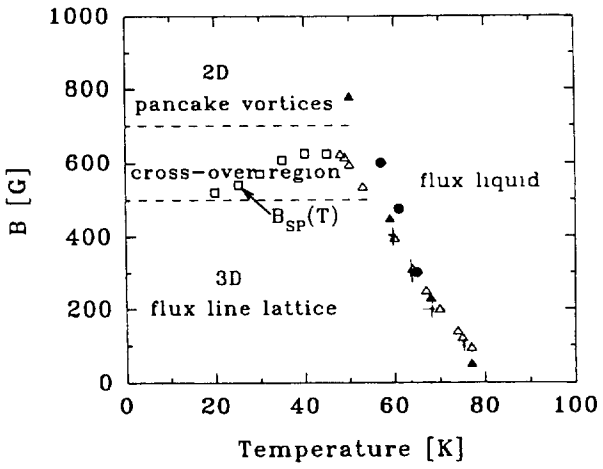

Fig. 15. — Comparison of the low field phase diagram obtained by three different techniques: muon spin rotation (solid triangles), neutron scattering (solid circle) and local Hall sensors (open triangles and squares) for Bi1.

determined in [37], significantly deviates from the FOT line in Bi1, but falls within the range determined by the Bi1 and Bi2 results.

Regarding the low-temperature part of the phase diagram, it is seen that the position of the second peak coincides with the crossover region determined by the μ^+SR and SANS experiments. It is therefore tempting to conclude that these features probe the same phenomenon, the more, because in all cases there is clear evidence that this phenomenon is related to the effect of point disorder (pinning). For instance, the asymmetry parameter α which follows from the μ^+SR work, changes in magnitude in the crossover region. In addition, the line width above the crossover field does not change substantially, and remains of the order of the width for an ideal lattice, see Section 2. Very recent theoretical work by Koshelev *et al.* [72] which deals with the effect of point disorder, is in good agreement with these features. Another observation in favor of the involvement of point disorder with respect to the origin of the second peak, is the small downward shift of $B_{sp}(T)$ after electron irradiation at low temperatures (20 K) [73]. This finding suggests that also in the non-irradiated crystals the position of the second peak, as well as the downward curvature of the FOT just above the critical point, are driven by the intrinsic properties of the crystal, the intrinsic point disorder included. It is interesting to note that the $B_{sp}(T)$ line often shows an unexplained tendency to decrease with decreasing temperature, as shown in Figure 15. Since point disorder shifts this line down, this behavior could be understood in terms of the increasing role disorder plays with lower temperatures. The existence of the second peak transition in the limit of vanishing disorder is still an open question which may help resolve the intriguing mystery of the mechanism behind the second peak.

4.4. Dynamic Probes of Vortex Lattice Melting in Bi-2212. — In the previous section we concluded that above the first order transition (FOT) line the flux line lattice is decomposed into pancake vortices. Nevertheless, it has not been decided whether the FOT represents a melting transition or not. Vortex lattice melting is characterized by a sudden decrease of the shear modulus c_{66} to zero. Ideally, such an effect should be probed by the disappearance of a

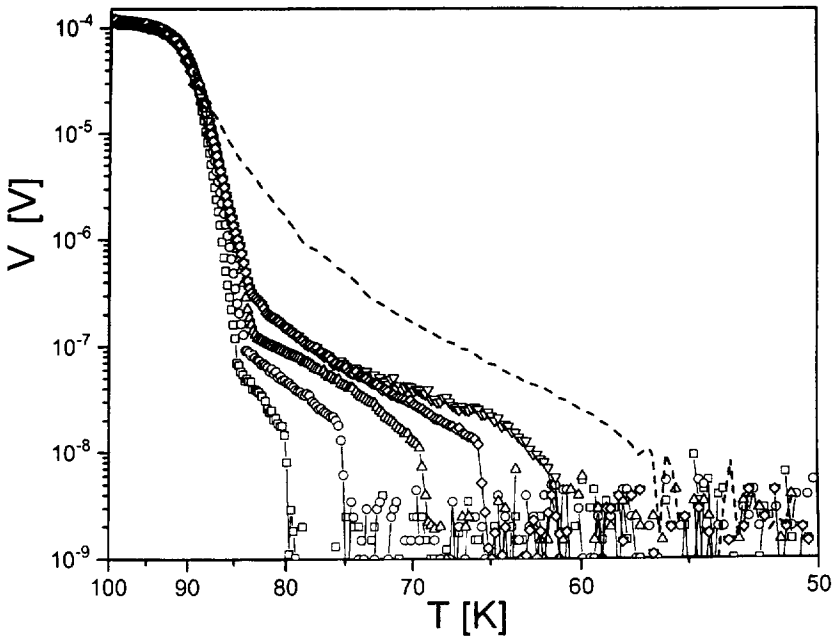

Fig. 16. — Arrhenius plot of voltage *vs.* temperature for a Bi-2212 single crystal with alternating strong pinning and weak pinning strips of approximately 12 μm and 3 μm width, respectively. Strong pinning areas are produced by heavy ion irradiation through a mask, dose 5×10^{10} cm^2 [73]. The dc transport current density was 1×10^2 A/cm^2 and fields of 100 Oe (□), 200 Oe (0), 300 Oe (△), 400 Oe (◇) and 500 Oe (▽ were applied. For comparison the Arrhenius plot for the sample before irradiation at 500 Oe is given as well (dashed line).

transverse "sound" wave in the vortex lattice. Alternatively, one may look at the disappearance of the flow stress τ in the lattice, since $\tau \propto c_{66}$. Such an experiment has been reported in reference [74] on an overdoped Bi-2212 single crystal, similar to Bi1. This crystal was partially masked and irradiated with heavy ions, which resulted in alternating strong pinning areas with columnar defects parallel to the *c*-axis, and weak pinning channels of approximately 3 μm width. By measuring the flux-flow voltage across the channels as a function of temperature at constant field and an appropriate constant current density ($\approx 1 \times 10^6$ A/m^2), the flow behavior of the vortex lattice has been probed. The main results are summarized in Figure 16, for details, we refer to [74]. The dashed line displays the usually observed broad resistive in-field transition of the sample before irradiation [4]. The open symbols show the results of the same sample after (partial) irradiation for fields between 100 Oe and 500 Oe. These fields are much smaller than the dose-equivalent field of 1 T which determines the density of columnar defects. Between the voltage contacts the total length of the irradiated area with strong pinning is about 20 times larger than the accumulated width of the channels. This geometry assures that the sharp voltage drop at high temperature is associated with the thermally activated depinning of vortices, trapped by the columnar defects. Below the temperatures where a sharp kink is observed, only the vortices inside the non-irradiated channels are moving. In this temperature regime the only mechanism that impedes the vortex motion is the usual Bardeen-Stephen friction and the shear viscosity of the vortex liquid [75]. As soon as the liquid freezes the shear interaction sets in which results in a voltage drop at the freezing temperature T_m. Actually, the

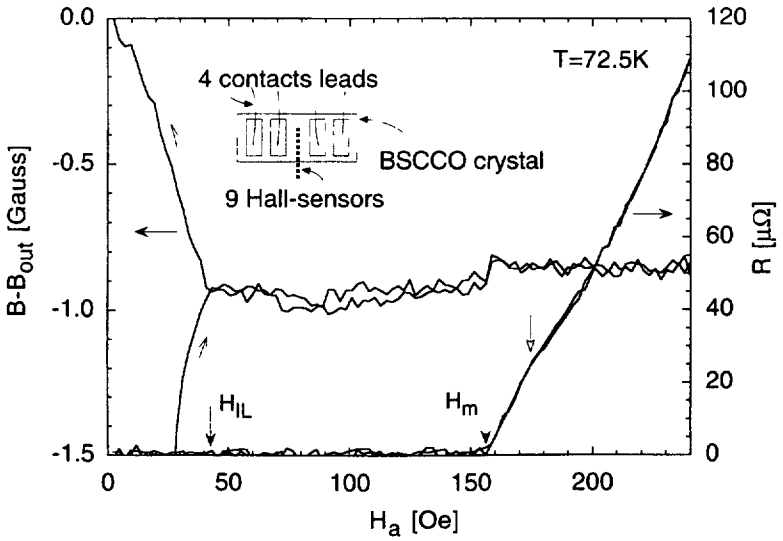

Fig. 17. — Simultaneous resistance and local magnetization measurements of BSCCO crystal as a function of increasing and decreasing applied field H_a. The first-order thermodynamic magnetization step coincides with the resistive onset at the phase transition H_m. The inset shows the experimental configuration.

temperature of the drop may be slightly higher then the thermodynamic melting temperature T_m, because the shear viscosity grows very fast upon approaching T_m from above. Using a 2D model, $\eta \propto \exp[b(T_m/(T - T_m))^\nu]$ with $\nu = 0.36963$ [76], it is estimated that the real T_m is between 1.5 K (at 100 Oe) and 0.5 K (at 400 Oe) lower than the temperature at the voltage drop [77].

When the results of the channel experiments are plotted in one $B - T$ diagram together with the μ^+SR, SANS and Hall sensor results on Bi1, it is seen that all data coincide within experimental accuracy. This observation demonstrates that all experimental techniques probe the same physical feature. On the one hand the channel experiment proves that the FOT is a first order *melting* transition (see also below). On the other hand the SANS results are clearly indicating a *decoupling* transition (see Sect. 4.3). (The ac-experiments of Pastoriza *et al.* [37] also favours a decoupling interpretation, but these results cannot be quantitatively compared to ours since they were obtained on a Bi-2212 crystal of unknown oxygen content.) The coincidence of all data thus give strong support to a combined metling-decoupling transition, or melting induced decoupling. Therefore, one should speak of a *sublimation* rather than a melting transition, since the vortex solid transfers into a gas of point vortices [73].

The simultaneous detection of the local flux density and global resistivity reveals a sharp onset of flux flow at the same field where a step in the magnetization occurs [78]. This is shown in Figure 17 for as-grown Bi-2212 at $T = 72.5$ K in an applied transport current density of ≈ 100 A/cm^2. The geometry of the experimental set up is sketched as well. Most experiments were carried out on a crystal with contacts on the top surface, but no significant differences were seen for side contacts. The sharp onset of the flux flow resistivity is quite remarkable, since one usually observes a smooth transition. But very similar features have been seen on a low-resistivity crystal of different origin. The coincidence of the FOT and the resistance onset is convincingly demonstrated in Figure 18. It strongly suggests that flux flow is triggered by the

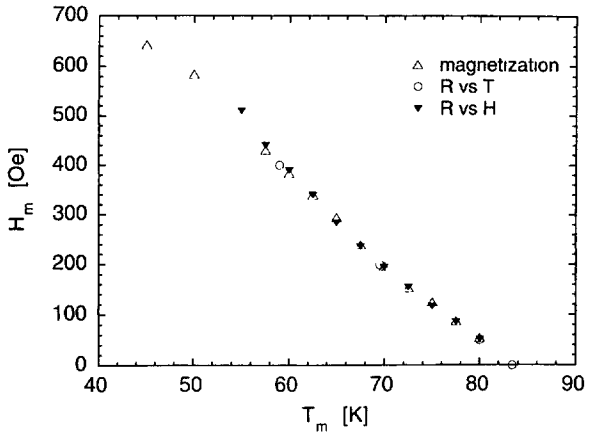

Fig. 18. — The first-order phase transition line of BSCCO crystal at elevated temperatures. The transition line is composed of data from three different measurements: (△) local magnetization *vs.* H_a (see Fig. 17), (▽) resistance *vs.* H_a and (○) resistance *vs.* T. The coinciding data show that the resistive transition is determined by the vortex-lattice phase transition.

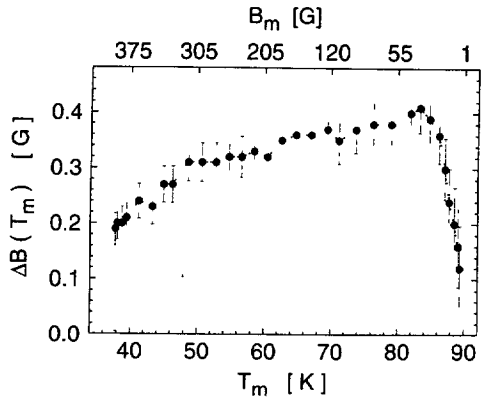

Fig. 19. — The height of the flux density step at the FOT line of an as-grown Bi-2212 single crystal. The step disappears abruptly at a critical point at about 38 K.

FOT. Above the phase transition linear $V - I$ characteristics are reported [78] with thermally activated resistivity, possibly originating from surface barriers for pancake vortices [70, 79]. This and the disappearance of bulk and or surface pinning at the FOT is once more in favor of the sublimation scenario.

4.5. THERMODYNAMICS OF THE FIRST-ORDER PHASE TRANSITION. — In this final section the thermodynamic consequences of the FOT are discussed [36]. Figure 19 shows the height of the step in the local induction along the FOT line. Quite remarkable is the sudden disappearance of the step indicating a critical point at 37.8 K and 380 G. The step height is monotonically increasing with T_m upto a maximum value of about 0.4 G at $\approx$ 83 K and drops rapidly near T_c.

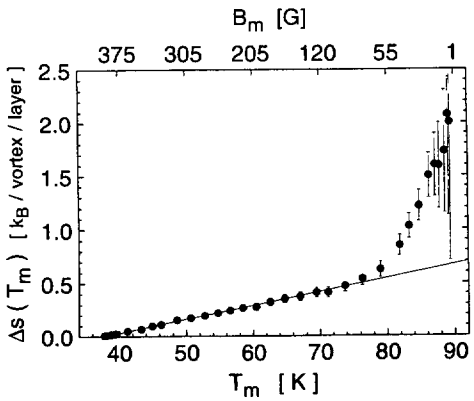

Fig. 20. — Entropy change per pancake vortex deduced from the flux density step shown in the previous figure as a function of temperature and field (upper scale). The entropy change vanishes linearly with T at the critical point. A strong increase is seen near T_c.

Using the Claussius-Clapeyron relations the entropy change at the transition and the latent heat per unit volume can be calculated from

$$\Delta S = -\frac{\Delta B}{4\pi}\frac{\mathrm{d}H_m}{\mathrm{d}T} \qquad L = T_m \Delta S \tag{11}$$

The entropy change per pancake vortex is therefore given by

$$\Delta s = -\frac{\mathrm{d}\phi_0}{4\pi}\frac{\Delta B}{B_m}\frac{\mathrm{d}H_m}{\mathrm{d}T} \tag{12}$$

where $d(= 1.54$ nm) is half the size of the crystallographic unit cell in the c-direction. Since $B_m(T) > H_{c1}(T)$, the slope of the melting line can be expressed in terms of the directly measured $\mathrm{d}B_m/\mathrm{d}T$. The resulting $\Delta s(T_m)$ is shown in Figure 20. Close to T_c the entropy change per vortex increases rapidly which could be related to critical fluctuations. This diverging behavior of Δs has been confirmed recently by more accurate local ac measurements [82]. At lower temperatures, $T_m < 75$ K, Δs decreases linearly with decreasing temperature and vanishes at the critical point. This is not related to a vanishing of ΔB, as would be expected, but is caused by the flattening of the FOT line here (see Fig. 14), which makes $\mathrm{d}B_m/\mathrm{d}T$ go to zero. The existence of the critical point is possibly disorder-related. Very recent SANS data with much better statistics than those reported in Section 3, shows that at high fields the melting line does not go horizontal at low temperatures, but continues upward [80].

Estimates for ΔB and ΔS can be obtained from a simple Lindemann melting scenario leading to [36] $\Delta s \approx 0.1\gamma \mathrm{d}k_B(B_m/\phi_0)^{1/2}$ and $\Delta B \approx -k_B\gamma(B_m/\phi_0)^{3/2}(\mathrm{d}B_m/\mathrm{d}T^{-1})$ At 70 K these expressions result in order of magnitude too low values of both ΔB and Δs. In addition, the temperature dependence of both quantities are not correctly predicted. It should be noted that 70 K is high enough that the effect of disorder can be neglected and low enough that critical phenomena play no role. The decoupling scenario gives rise to a temperature independent estimate $\Delta s \approx 0.5k_B$ in good agreement with Monte-Carlo simulations which gave $\Delta s \approx 0.3k_B$ [81]. It also leads to a linearly increasing $\Delta B \propto (1 - t_m)$ which at $T = 70$ K reaches a value $\Delta B(70\ \mathrm{K}) \approx 0.4$ G. Both values agree reasonably well with the values observed at 70 K in Figures 19 and 20, but it is clear that the expected temperature dependences are

not observed. This lack of fully understanding the thermodynamics of the FOT calls for new, high precision experiments. It also makes this subject a remaining source of inspiration for theoreticians.

5. Summary and Conclusions

In this contribution recent experiments are reviewed which explore the low-field phase diagram of the Bi-2212 compound with a variety of quite different techniques. They are presented here in a more or less sequential way in order to sketch the developments over the last few years. An interesting point to note is that many of these experiments have been carried out on single crystals of the same origin. They were prepared, grown and heat-treated identically. This is an important prerequisite for consistency checks and a true comparison of the different results. It is by no means trivial, because the relevant properties of this compound sensitively depend on the oxygen stoichiometry. The picture that emerges from the experiments, is summarized in the Figures 14 and 15. In Figure 14 the Hall sensor results for three single crystals with different oxygen content are plotted in the same $B - T$ diagram. The effect of oxygen stoichiometry is obvious. At high temperatures the data represent the first-order transition lines determined by a discontinuous increase in the local induction. These lines end in a critical point at about 40 K and then continue to lower temperatures as the three lines marking the positions of the second peak in the magnetization. In Figure 15 the results of the overdoped sample of the previous figure are compared with the μSR and SANS data. It is seen that the FOT line coincides with characteristic features observed with μSR and SANS. At low temperatures the second peak line is seen to coincide with a crossover from 3D to 2D behavior detected by the internal field probes. Combining these observations with the results of transport measurements, it is concluded that at the FOT line the vortex lattice sublimates into a gas of pancake vortices. The nature of the crossover at high fields and the underlying mechanism are still unresolved. It is clear, however, that disorder plays a crucial role here. According to a suggestion by several authors [83] the crossover may actually be a disorder driven true thermodynamic phase transition which is characterized by the proliferation of dislocations in the pinned vortex lattice (low field) transforming it into an amorphous vortex glass of individually pinned pancake vortices (high field). Probably, disorder is also responsible for the flattening of the FOT line on approaching the critical point. The exact temperature dependence of the FOT line and the magnitude of the steps in local induction and entropy are not yet satisfactorily explained.

Acknowledgments

The various projects reviewed in this paper were supported by the U.K. Science and Engineering Research Council, The U.S. Department of Energy, the Large Installation Programme of the EU, The Swiss National Science Foundation, the Glikson Foundation, the Minerva Foundation, the French-Israel Cooperation Programme (AFIRST), the U.S.-Israel Binational Foundation, The Ministry of Education, Science and Culture of Japan, Contract CT1*CT930063 of the EU, and the Dutch Foundation for Fundamental Research on Matter (FOM).

References

[1] Bishop D.J., *Nature* **365** (1993) 394.
[2] Nelson D.R., *Nature* **375** (1995) 356.

[3] Abrikosov A.A., *Sov. Phys. JETP* **5** (1957) 1174.
[4] Palstra T.T.M., Batlogg B., Schneemeyer L.F. and Waszczak J.W., *Phys. Rev. Lett.* **61** (1988) 1662.
[5] Koch R.C., Foglietti V., Gallagher W.J., Koren G.,Gupta A. and Fisher M.P.A., *Phys. Rev. Lett.* **63** (1989) 1511.
[6] Muller K.A., Takashige M. and Bednorz J.G., *Phys. Rev. Lett.* **58** (1987) 1143.
[7] Yeshurun Y. and Malozemoff A.P., *Phys. Rev. Lett.* **60** (1988) 2202.
[8] Yeshurun Y., Malozemoff A.P.,Holtzberg F. and Dinger T.R., *Phys. Rev. B* **38** (1988) 11828.
[9] Wolfus Y., Yeshurun Y. and Felner I., *Phys. Rev. B* **39** (1989) 11690.
[10] Kopylov V.N., Togonidze T.G. and Schegolev I.F., *Physica C* **195** (1992) 379; *Physica C* **162-164** (1989) 1143.
[11] Feigel'man M.V., Geshkenbein V.B. and Larkin A.I., *Physica C* **167** (1990) 177.
[12] Feigelman M.V. and Vinokur V.M., *Phys. Rev. B* **41** (1990) 8986.
[13] Vinokur V.M., Kes P.H. and Koshelev A.E., *Physica C* **168** (1990) 29.
[14] Bulaevskii L.N., Kolesnikov N.N., Schegolev I.F. and Vyaselev O.M., *Phys. Rev. Lett.* **71** (1993) 1891.
[15] Fisher D.S., Fisher M.P.A. and Huse D.A., *Phys. Rev. B* **43** (1991) 130.
[16] Fisher M.P.A., *Phys. Rev. Lett.* **62** (1989) 1415.
[17] Huse D.A., Fisher M.P.A. and Fisher D.S., *Nature* **358** (1992) 553.
[18] Bishop D.J., Gammel P.L., Huse D.A. and Murray C.A., *Science* **255** (1992) 165.
[19] Nelson D.R., *Phys. Rev. Lett.* **60** (1988) 1973.
[20] Houghton A., Pelcovits R.A. and Sudbo A., *Phys. Rev. B* **40** (1989) 6763.
[21] Brandt E.H., *Phys. Rev. Lett.* **63** (1989) 1106.
[22] Hikami S., Fujita A. and Larkin A.I., *Phys. Rev. B* **44** (1991) 10400.
[23] Blatter G. and Ivelev B.I., *Phys. Rev. B* **50** (1994) 10272.
[24] Huberman B.A. and Doniach S., *Phys. Rev. Lett.* **43** (1979) 950; Fisher D.S., *Phys. Rev. B* **22** (1980) 1190.
[25] Kosterlitz J.M. and Thouless D.J., *J. Phys. C* **6** (1973) 1106; Kosterlitz J.M., *J. Phys. C* **7** (1974) 1046.
[26] Young A.P., *Phys. Rev. B* **19** (1979) 1855.
[27] Halperin B.I. and Nelson D.R., *Phys. Rev. B* **19** (1979) 2457.
[28] Bishop D.J., Gammel P.L., Waszczak J.V. and Schneemeyer L.F., *Bull. Am. Phys. Soc.* **33** (1988) 606.
[29] Gammel P.L., Schneemeyer L.F., Waszczak J.V. and Bishop D.J., *Phys. Rev. Lett.* **61** (1988) 1666.
[30] Blatter G., Feigel'man M.V., Geshkenbein V.B., Larkin A.I. and Vinokur V.M., *Rev. Mod. Phys.* **66** (1994) 1125.
[31] van der Beek C.J. and Kes P.H., *Phys. Rev. B* **43** (1991) 13032.
[32] Brezin E., Nelson D.R. and Thiaville A., *Phys. Rev. B* **31** (1985) 7124.
[33] Safar H. *et al., Phys. Rev. Lett.* **69** (1992) 824; *Phys. Rev. Lett.* **71** (1993) 436.
[34] Kwok W.K. *et al., Phys. Rev. Lett.* **69** (1992) 3370; *Phys. Rev. Lett.* **72** (1994) 1092; Charalambous M. *et al., Phys. Rev. Lett.* **71** (1993) 436.
[35] Jiang W., Yeh N.-C., Reed D.S., Kriplani U. and Holtzberg F., *Phys. Rev. Lett.* **74** (1994) 1438.
[36] Zeldov E., Majer D., Konczykowski M., Geshkenbein V.B., Vinokur V.M. and Shtrikman H., *Nature* **375** (1995) 373.
[37] Pastoriza H., Goffman M.F., Arribere A. and de la Cruz F., *Phys. Rev. Lett.* **72** (1994) 2951.

[38] Lee S.L., Zimmermann P., Keller H., Warden M., Savıc I.M., Schauwecker R., Zech D., Cubitt R., Forgan E.M., Kes P.H., Li T.W., Menovsky A.A. and Tarnawski Z., *Phys. Rev. Lett.* **71** (1993) 3862.
[39] Cubitt R., Forgan E.M., Yang G., Lee S.L., Paul D.Mck., Mook H.A., Yethiraj M., Kes P.H., Li T.W., Menovsky A.A., Tarnawski Z. and Mortensen K., *Nature* **365** (1993) 407.
[40] Majer D., Zeldov E., Shtrikman H. and Konczykowski M., ın Coherence in High-T_c Superconductors (World Scientific, Singapore, 1996) (in press).
[41] Seeger A., *Phys. Lett.* **77A** (1979) 259.
[42] Brandt E.H. and Seeger A., *Adv. Phys.* **35** (1986) 189.
[43] Li T.W., Kes P.H., Hien N.T., Franse J.J.M. and Menovsky A.A., *J. Crystal Growth* **135** (1994) 481.
[44] Rainford B.D. and Daniell G.J., in: Proceedings of the 6th International Conference on Muon Spin Rotation, Relaxation and Resonance (Hawaii, 1993).
[45] Brandt E.H., *J. Low Tem. Phys. Vol.* **73** (1988) 355.
[46] Harshman D.R., Kleiman R.N., Inui M., Espinosa G.P., Mitzi D.B., Kapitulnik A., Pfiz T. and Williams D.Ll., *Phys. Rev. Lett.* **67** (1991) 3152.
[47] Harshman D.R., Brandt E.H., Fiory A.T., Inui M., Mitzi D.B., Schneemeyer L.F. and Waszczak J.V., *Phys. Rev. B* **47** (1993) 2905.
[48] Barford W. and Gunn J.M.F., *Physıca C* **156** (1988) 515.
[49] Brandt E.H., *Phys. Rev. Lett.* **66** (1991) 3213.
[50] Martinez J.C., Brongersma S.H., Koshelev A.E., Ivlev B., Kes P.H., Griessen R.P., de Groot D.G., Tarnavski Z. and Menovsky A.A., *Phys. Rev. Lett.* **69** (1992) 2276.
[51] Cubbit R., Forgan E.M., Warden M., Lee S.L., Zimmermann P., Keller H., Savıc I.M., Wenk P., Zech D., Kes P.H., Li T.W., Menovsky A.A. and Tarnawski Z., *Physıca C* **213** (1993) 126.
[52] Song Y.-Q. *et al., Phys. Rev. Lett.* **70** (1993) 3127.
[53] de Gennes P.G. and Matricon J., *Rev. Mod. Phys.* **36** (1964) 45.
[54] Criber D. *et al., Phys. Lett.* **9** (1964) 106.
[55] Forgan E.M., Paul D.Mck., Mook H.A., Timmins P.A., Keller H., Sutton S. and Abell J.S., *Nature* **343** (1990) 735.
[56] Forgan E.M. *et al., Physıca C* **185-189** (1991) 247.
[57] Yethiraj M. *et al., Phys. Rev. Lett.* **70** (1993) 857.
[58] SudbøA. and Brandt E.H., *Phys. Rev. Lett.* **66** (1991) 1781.
[59] Glazman L.I. and Koshelev A.E., *Phys. Rev. B* **43** (1991) 2835.
[60] van der Beek C.J., Kes P.H., Maley M.P., Menken M.J.V. and Menovsky A.A., *Physıca C* **185-189** (1991) 2507; van der Beek C.J., Ph.D. thesis, Leiden Universıty (1992).
[61] Christen D.K., Tasset F., Spooner S. and Mook H.A., *Phys. Rev. B* **15** (1977) 4506.
[62] Zeldov E., Larkin A.I., Geshkenbein V.B., Konczykowski M., Majer D., Khaykovıch B., Vinokur V.M. and Shtrikman H., *Phys. Rev. Lett.* **73** (1994) 1428.
[63] Brandt E.H. and Indenbom M., *Phys. Rev. B* **48** (1993) 12893.
[64] Li T.W., Menovsky A.A., Franse J.J.M. and Kes P.H., *Physica C* **257** (1996) 179.
[65] Khaykovıch B., Zeldov E., Majer D., Li T.W., Kes P.H. and Konczykowski M., *Phys. Rev. Lett.* **76** (1996) 2555.
[66] Motohira N. *et al., J. Ceram. Soc. Jpn Int. Ed.* **97** (1989) 994.
[67] Nelson D.R., Ice-like melting of flexible line crystals, Paper presented at the Indo-US Symposium on "Liquıd Crystals and Supramolecular Order", Bangalore, Jan. 2-5, 1996. To appear ın Molecular Crystals and Liquid Crystals.
[68] Daemen L.L., Bulaevskii L.N., Maley M.P. and Coulter J.Y., *Phys. Rev. Lett.* **70** (1993) 1167; *Phys. Rev. B* **47** (1993) 11291.

[69] Blatter G., Geshkenbein V., Larkin A. and Nordborg H., *Phys. Rev. B* **54** (1996).
[70] Kopylov V.N., Koshelev A.E., Schegolev I.F. and Togonidze T.G., *Physica C* **170** 291 (1990).
[71] Kishio K., Shimoyama J., Kotaka Y. and Yamafuji K., in "Proc. 7th Intnl. Workshop on Critical Currents in Superconductors", H.W. Weber Ed. (World Scientific Pub., Singapore, 1994) p. 339.
[72] Koshelev A.E., Glazman L.I. and Larkin A.I., *Phys. Rev.* **B53** (1996) 2786.
[73] Khaykovich B., Konczykowski M., Zeldov E., Doyle R.A., Kes P.H., Majer D. and Li T.W., submitted.
[74] Pastoriza H. and Kes P.H., *Phys. Rev. Lett.* **75** (1995) 3225.
[75] Marchetti C. and Nelson D.R., *Phys. Rev. B* **42** (1990) 9938.
[76] Nelson D.R. and Halperin B.I., *Phys. Rev. B* **19** (1979) 2457.
[77] Theunissen M.H. and Kes P.H., *Phys. Rev. Lett.* **77** (1996) 159.
[78] Fuchs D.T., Zeldov E., Majer D., Doyle R.A., Tamegai T., Ooi S. and Konczykowski M., *Phys. Rev. B* **54** (1996) R796.
[79] Hagen C.J. *et al.*, private communication.
[80] Forgan E.M., private communication.
[81] Hetzel R.E., Sudbø A. and Huse D., *Phys. Rev. Lett* **69** (1992) 518.
[82] Morozov N., Zeldov E. and Majer D., *Phys. Rev. B* (in press).
[83] Giamarchi T. and Le Doussal P., *Phys. Rev.* **B52** (1995) 1242; Gingras M.J.P. and Huse D.A., *Phys. Rev. B* **53** (1996) 15193; Kierfeld J., Nattermann T. and Hwa T., submitted; Ertas D. and Nelson D.R., submitted.